Hindawi
Advances in Materials Science and Engineering
Volume 2018, Article ID 9512957, 12 pages
https://doi.org/10.1155/2018/9512957

Research Article

Influence of Thermal Parameters, Microstructure, and Morphology of Si on Machinability of an Al–7.0 wt.% Si Alloy Directionally Solidified

Cássio A. P. Silva,[1] Layo R. M. Leal,[1] Emanuelle C. Guimarães,[1] Paulo M. Júnior,[1] Antonio L. Moreira,[1] Otávio L. Rocha,[2] and Adrina P. Silva[1]

[1]*Federal University of Pará, Augusto Correa Avenue 01, P.O. Box 479, Belém, PA, Brazil*
[2]*Federal Institute of Education, Science and Technology of Pará, Almirante Barroso Avenue 1155, P.O. Box 66093-020, Belém, PA, Brazil*

Correspondence should be addressed to Adrina P. Silva; mariaestillac@gmail.com

Received 16 August 2017; Accepted 20 February 2018; Published 3 April 2018

Academic Editor: Patrice Berthod

This study aims to correlate the influence of thermal and microstructural parameters such as growth rate and cooling rate (V_L and T_R) and secondary dendrite spacing (λ_2), respectively, in the machining cutting temperature and tool wear on the necking process of the Al–7 wt.% Si alloy solidified in a horizontal directional device using a high-speed steel with a tungsten tool. The dependence of λ_2 on V_L and T_R and dependence of the maximum cutting temperature and maximum flank wear on λ_2 were determined by power experimental laws given by $\lambda_2 = \text{constant}\ (V_L \text{ and } T_R)^n$ and T_{MAX}, $V_{BMAX} = \text{constant}\ (\lambda_2)^n$, respectively. The maximum cutting temperature increased with increasing of λ_2. The opposite occurred with the maximum flank wear. The role of Si alloying element on the aforementioned results has also been analyzed. A morphological change of Si along the solidified ingot length has been observed, that is, the morphology of Si in the eutectic matrix has indicated a transition from particles to fibers along the casting together with an increase of the particle diameters with the position from the metal/mold interface.

1. Introduction

It is well known that machining is one of the most important manufacturing processes in the metal-mechanical industry [1]. The improvement in the machining operation is related to obtaining components with the desired dimensions and satisfactory surface quality. In addition, large increases in productivity can be achieved. The economic advantages of the right choice of material to be machined, as well as the tools, cutting fluid, equipment, and machining conditions are considerable. The costs and production times can be significantly reduced by choosing the right parameters [2].

The total work done by the cutting tool in the metal removal can be determined from the values of the force components on the cutting tool. Approximately, all of this work or energy is converted into heat, which is dissipated to the tool material and the machined piece. For greater forces on the tool, more work is required on the removal of metal, which in turn affects the temperature [3].

The fact that machining temperature has a critical influence on tool wear and tool life has been well recognized since Taylor's work in 1907 [4]. In particular, the rate of crater formation is very dependent on the temperature at tool interface. The crater wear growth at the tool interface has been found and is directly regulated by the temperature distribution along the interface. For the above reasons, the problem of determining the machining temperature has been extensively researched over the years. Many experimental techniques have been applied for the measurement of the processing temperature; however, good accuracy is difficult to achieve [5, 6].

Although the main reason for continued temperature measurement work is to improve the quality of the finished part, and it can also help predict tool wear and the development of predictive modeling software. In addition, studies

have shown that, in material removal processes, a phenomenon that can degrade the quality of the piece, they often follow an Arrhenius model (exponential type), implying that some otherwise incompatible behaviors can actually be attributed to variations of temperature [7].

There is no general consensus about the results obtained by several authors using the various temperature measurement techniques available. The complexity of the machining process makes it extremely difficult to compare the results of different techniques. This difficulty is illustrated by the fact that the results obtained are different because there are different ways of measuring the experiments, even if performed under the same cutting conditions and in the same tool and materials. Even so, the radiation technique has many advantages, including fast response, no adverse effects on temperatures and raw materials, without physical contact, and allowing measurements on objects that are difficult to access. However, the position measurement has to be carefully selected because the accuracy can be significantly affected by the obstruction. The tool obstruction also makes it difficult to measure the temperature at the tool interface [8].

With regard to cutting tools, tool wear is caused by a number of factors, whether the machining conditions to which this tool is subjected (cutting speed, feed, and depth of cut) and geometry thereof or the composition of the alloy, type of carbides, and structure formed after solidification. The types of wear are flank, notch, and crater, with crater and flank wear being the most regular and predictable ways [9]. In the literature, different nomenclatures and treatments for tool wear mechanisms are found. Trent and Wright [4], for example, define six mechanisms or wear processes: plastic shear at high temperatures, deformation under compressive stress, diffusion wear, adhesive and entrainment wear (attrition), abrasive wear, and notch wear. Although the notch wear is a form of wear, it is regarded as a mechanism due to lack of unanimity on their causes.

In tool material types, high-speed steel (HSS) stands out. The advantages of using high-speed steel tools are toughness, high resistance to breakage, and a lower price compared to other materials [10]. As with all other steels, alloying elements produce numerous effects on the properties of the high-speed steels. AISI T6, for example, has carbon and vanadium as elements directly responsible for wear resistance and high hot hardness; tungsten, molybdenum, and cobalt as elements that improve cutting properties and also increase the hardness at elevated temperatures; and chromium as the element which has the property of improving the oxidation resistance and the secondary hardening [11].

1.1. Machinability. The term machinability may be taken to imply that there is a property or quality of any given material which can be clearly defined and quantified, thus indicating how easy (or difficult) that mechanical operation can be. In fact, that term is not unambiguous, but the machinability of a material can be assessed by employing criteria such as (i) tool life or limiting rate of metal removal, (ii) surface finish and chip morphology, and (iii) cutting forces or power consumption [12]. Machinability can be compared by different ways and is determined by several different types of tests, like cutting forces, cutting temperatures, tool wear, and surface roughness [13].

The best performance of the machining operations sought by the professionals involved in the area (both researchers and professionals in the machining area) can be obtained through research involving materials and their structures since the control of these already in the process of solidification significantly reduces costs with further processing [14]. The operational parameters involved in the liquid/solid transformation, such as alloy system, alloy composition, overheating, mold temperature, mold material, heat transfer coefficient at the metal/mold interface, size of the piece, convection on the liquid phase, solute transport, and concentration of nucleating particles in the liquid, vary according to the considered process. These parameters influence the thermal conditions in which the phenomenon occurs, such as the displacement velocity of the *liquidus* isotherm (V_L), temperature gradient (G_L), and cooling rate (T_R), which depend both on time and position relative to the metal/mold interface [14–17]. Such transient conditions, as well as the different compositions of the alloys, lead to various possibilities of obtaining final structures for the same melt and, consequently, for their mechanical performance.

1.2. Al–Si Alloys: Industrial Importance and Morphology. It is well known that aluminum-silicon alloys are of a great industrial importance. These alloys are becoming the most popular aluminum alloys being used in tile automotive industry mainly due to their high strength to weight ratio, high castability, high corrosion, and wear resistance, as well as their high tensile, impact, and fatigue properties after a proper heat treatment [15, 18–21]. The manufacturing of piston for internal combustion engines, for instance, is made using hypoeutectic, eutectic, and hypereutectic aluminum-silicon alloys.

The range of silicon may roughly vary from 7 to 18 wt.%. Al–Si-based engine blocks, for instance, have a very complex geometry to be achieved. Such parts have to be initially cast and thereafter subject to machining. Many variables influence mechanical properties of Al–Si casting alloys, including chemical composition of the alloy, metal soundness in terms of gas and shrinkage porosity and inclusions, solidification conditions (or cooling rate), metallurgical characteristics including grain size, dendrite arm spacing (DAS), and the shape, size, and distribution of constituents, and applied heat treatment. The refinement of the microstructure leads to substantial improvement in mechanical properties. The secondary dendrite arm spacing controls the size and the distribution of porosity and intermetallic particles in the casting. Chemical composition, melting process, casting process, and solidification rate determine the quality of the microstructure of aluminum parts. As DAS becomes smaller, porosity and second phase constituents are dispersed more finely and evenly which also enhances the mechanical properties [20–22].

It is well established that under most conditions of solidification, the dendritic morphology is the dominant characteristic of the microstructure of off-eutectic alloys.

Fine dendritic microstructures in castings, characterized by the dendrite arm spacing, are recognized to have superior mechanical properties than coarser ones, particularly when considering the tensile strength and ductility. A eutectic constituent, comprising of aluminum-rich and silicon phases grows between the aluminum-rich dendritic networks [23].

When a hypoeutectic Al–Si alloy solidifies, the primary aluminum forms and grows in dendrites or silicon phase forms and grows in angular primary particles. When the eutectic point is reached, the eutectic Al–Si phases nucleate and grow until the end of solidification. At room temperature, hypoeutectic alloys consist of a soft and ductile primary aluminum phase and a hard and brittle eutectic silicon phase [19]. A dendritic arrangement of the primary Al-rich phase is quite common to be observed. Dendrites of faceted materials in Si, so-called "faceted dendrites" are distinguished from those of nonfaceted materials in metals and alloys [23]. Dendrite arm spacing as well as the size of Si particles, that is, microstructure scale, strongly depends on solidification behavior. The mechanical properties of the casting may be improved through microstructural modification, in which a refined fibrous silicon structure is obtained in lieu of a coarse flake structure. Al–Si modification may be achieved through additions of trace impurity elements or increased solidification velocity [23].

Various microstructures of silicon are expected based on temperature gradients (G) and interface velocities (R). However, all commercial castings solidify in the regime of interface velocity and temperature gradient that forms flaky silicon, which is the general class of irregular eutectic observed in unmodified alloys. In three dimensions, silicon exists in the form of flakes, but in the two dimensions, it appears as rods [23].

Studies have been carried out to investigate the performance of various artificial neural network (ANN) training algorithms in the finite-element method (FEM) modeling of eutectic volume percentage, silicon volume percentage, silicon rod spacing, average length of silicon rods, and silicon rod diameter of Al–Si alloys [24–29]. Mazahery and Shabani used the LM algorithm in FEM modeling of the average length and diameter of silicon rods. The method couples thermal and solute diffusion. Knowing the volume fractions of the primary dendrite phase, silicon, and eutectic, the average length of the silicon rods can be related to the primary dendrite size based on simple geometric considerations [23].

Silicon (Si) particles are normally formed as particles or needles enveloping the dendritic matrix. However, modifiers like Na, Sr, and Sb can be added in order to modify the shape from needle-like to fiber-like. Lu and Hellawell [30] and Shabani and Mazahery [29] were the first researchers who carried out the TEM characterization and introduced the impurity-induced twinning theory, which states that chemical modifiers are adsorbed onto surface steps and kinks and poison the growing atomic silicon layers, thus preventing the attachment of silicon atoms to the crystal [23].

Although improvement in mechanical properties due to such modification is well known [23, 31], the effects of both size of silicon particles and their morphologies on machinability of Al–Si parts remain unknown. Thus, this understanding means a task to be accomplished by research teams in academy or industry [32].

1.3. The Role of Solidification Parameters and Morphology of Si on Machinability. It is now known that the conditions imposed during the liquid/solid transformation process, combined with the thermophysical properties of both the material and the mold, directly affect the mechanical properties of the cast products. Thus, it is essential to approach some methodologies used in the study of this phenomenon highlighting, for example, the directional solidification technique, which can be applied in both stationary conditions as for transient heat extraction, and this latter is what represents the most industrial processes. On this way, considerable research [16, 17, 33–36] has been made in recent decades in order to establish in a systematic way the influence of various operating parameters and thermal phenomena involved in the solidification on the resulting structure. They seek to raise the mechanical properties and, therefore, the performance of the materials solidified by experimental procedures, which have been performed in the vast majority in upward and downward vertical solidification systems.

Only a few studies, however, have reported correlations between structural characteristics and mechanical properties of solid when solidification occurs in a horizontal directional system [37, 38]. It is important to note that few studies attempt to relate structural features with machining temperatures, especially on aluminum alloys.

Recent study developed by Sokołowski et al. [39] has shown that in the case of high-speed milling (HSM) operations of Al–Si sand casting (under constant speed, feed, and axial depth of cut) surface roughness is a function of both the silicon content and morphology of the silicon phase. It has been demonstrated that an increase in the resultant cutting force degrades the machined surface finish.

Zedan et al. [40] selected T6 heat-treated 396 alloys (containing ~11 wt.% Si), and B319.2 and A356.2 alloys (containing ~7 wt.% Si) in order to perform drilling. It was found that alloys containing higher silicon content required greater cutting force for the same level of Mg and very close Brinell hardness values of about 108 HB. In terms of number of holes drilled, such results indicate that the silicon content has little effect on the tool life. They also stated that there is a need for bridging the boundary between casting process and machining operations, with a view of examining various aspects affecting the machinability of Al–Si casting alloys.

Turning is ubiquitous and is one of the most studied processes, with the measurement of process temperature being no exception. Based on this fact, Silva et al. [41] investigated the effect of solidification thermal parameters on the macrostructure of an Al–7 wt.% Si alloy during the horizontal directional solidification under unsteady-state heat flow conditions and its correlation with cutting temperatures. They have observed higher average cutting temperature for the columnar structure.

It is known that most of the work performed in metal machining process is converted into heat. Ductility, hardness, and thermal properties have significant effect on the acting forces, as well as on the generated temperatures, and these properties, together with the characteristics of the cutting tool material and conditions of machining process, define the cutting force and hence the heat generated and tool wear. It is also known that there are few studies that correlate structural features with machinability aspects, especially on aluminum alloys [39–41]. So, the purpose of this study is to analyze the necking process of an Al–7.0 wt.% Si ingot solidified on a directional solidification device, using an HSS T6 toll, correlating machinability aspects such as cutting temperature and tool wear with solidification microstructural aspects.

2. Experimental Procedure

The casting assembly used in solidification experiment was recently published [37, 38]. Its design allows heat extraction only through the water-cooled system placed in one of the lateral mold walls, waging horizontal directional solidification. The carbon steel mold used had a wall thickness of 3 mm, a length of 110 mm, a height of 60 mm, and a width of 80 mm. The lateral inner mold surfaces were covered with a layer of insulating alumina, and the upper part of the mold was closed with refractory material to prevent heat losses. The thermal contact condition at the metal/mold interface was also standardized with the heat-extracting surface being polished.

The experiment was carried out with an Al–7 wt.% Si alloy with superheat of 10% above the *liquidus* temperature, as shown in previous articles, as well as the enlarged partial phase diagram of the Al–Si system, which permits a clear visualization of phases and transformation temperatures in the hypoeutectic range of Al–Si alloys [42–44]. During the solidification process, temperatures at different positions in the alloy samples were measured and the data were acquired automatically, using a set of fine-type K thermocouples. The thermocouples were sheathed in 1.6 mm diameter steel tubes and positioned at 5, 10, 15, 30, and 50 mm from the heat-extracting surface. The thermocouples were calibrated at the melting point of Al, exhibiting fluctuations of about 0.4°C and 1°C, respectively, and connected by coaxial cables to a data logger interfaced with a computer. The experimental cooling curves for this experiment are shown in Figure 1(a).

It is well known that the dendritic arm spacings are dependent on the solidification thermal parameters such as V_L and T_R [20, 34], all of which vary with time and position during solidification. In order to determine parameters with more accurate values, the thermocouple readings were used to generate algebraic position expressions from the metal/mold interface as a function of time, that is, $P = f(t)$, corresponding to the *liquidus* front passage through the thermocouples. After determining the algebraic expressions of the position as a function of time, the experimental velocities of the *liquidus* isotherm (V_L) were calculated as a function of the position obtained through the derivative of the equation.

The cooling rate T_R for each position of the thermocouples was obtained experimentally from the intersections of the *liquidus* temperature line (T_L) with the thermal profile at each position of the thermocouples, through the direct reading of the quotient of the temperatures just before and after T_L and the corresponding times. The method used for measuring the tip cooling rate was detailed by Rocha et al. [45], and Figures 1(b) and 1(c) show both experimental growth and cooling rates as function of *liquidus* isotherm position, that is, $(V_L) = f(P)$.

The ingot was sectioned along its longitudinal direction, which is parallel to both the sample axis and the direction of solidification, and after this, it was mechanically polished with abrasive papers and subsequently etched with an acid solution composed of 5 ml H_2O, 60 ml HCl, 30 ml HNO_3, and 5 ml HF to reveal the macrostructure. A columnar-to-equiaxed transition (CET) was observed, as shown in Figure 2.

Selected longitudinal (parallel to the horizontal growth direction) sections of the directionally solidified specimens at 5, 10, 15, 20, 30, 40, 50, and 60 mm from the metal/mold interface were polished and etched with a solution of 0.5% HF in water for micrograph examination. Image processing system Olympus BX51 and Image Tool (IT) software were used to measure secondary dendrite arm spacings (λ_2). The λ_2 values were measured on the longitudinal section by averaging the distance between adjacent side branches [44]. Furthermore, microstructural characterization was performed using scanning electron microscopy.

The purpose of this study is to correlate machinability and microstructural aspects of an Al–7.0 wt.% Si alloy, such as λ_2 and Si morphology. As these aspects vary with the distance from metal/mold interface, it was necessary to carry out several neckings along the casting length. Necking is not usual for machining operations, but as there was no turning process to change the geometry of the cross section from rectangular to circular in order to avoid recrystallization and modification of the ingot macrostructure, the depth of the penetration adopted was the whole dimension of the section, characterizing necking process. This is a usual kind of machinability test [46].

Due to material losses that occur during the cutting process and to the thickness of the chisel, process vibrations, and so on, it was not possible necking at the same positions in which the spacing was measured. Thus, the longitudinal section of the ingot was divided in six workpieces with dimensions of the section to be machined from 14×17 mm, as shown in Figure 3(a), in the positions shown in Table 1. A refrigerated band saw was used to prepare the specimens.

Machining tests were carried out through necking assays, performed on a conventional lathe. The choice of conventional lathe is because of still wide application in an industrial scale. For the tool, it was used HSS T6 3/4″ conventional chisels with their original polishing and grinding.

Machining parameters are functions of many aspects, such as machining process, type of machine, type of material to be machined, and the cutting tool used. The cutting parameters related to both the machining process and type

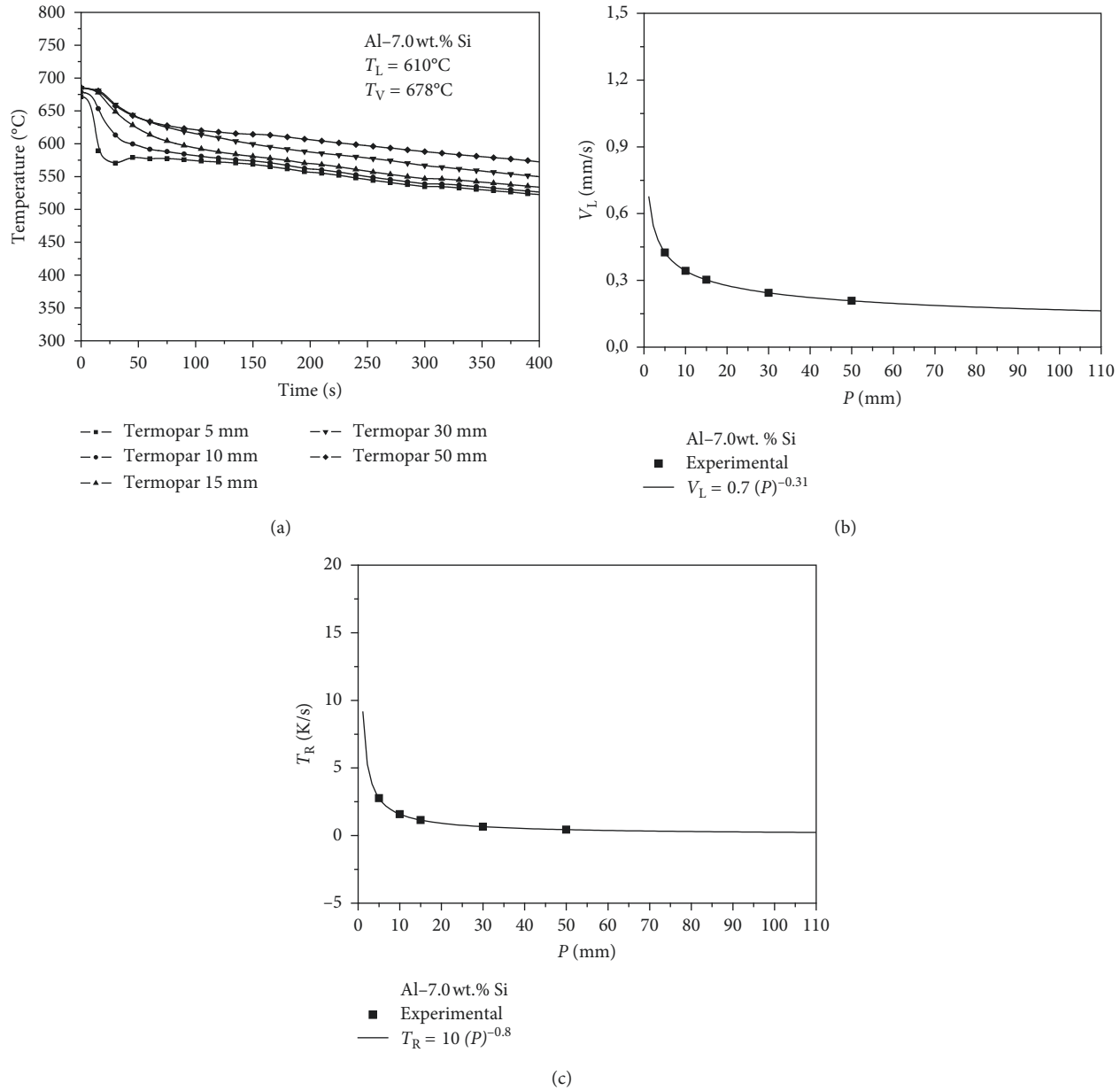

Figure 1: (a) Experimental cooling curves at different positions along the casting length during the directional solidification of Al–7.0 wt.% Cu alloy. T_L is the *liquidus* temperature; (b) and (c) growth rate and cooling rate as functions of *liquidus* isotherm position, respectively [43].

of machine are cutting speed, feed, and depth of cut. For the cutting tool, the involved parameters are material, shape, and geometry of the tool and for the material to be machined are chemical composition, hardness, and surface treatment. With the union of the parameters (machining processes, type of machine, cutting tools, and material), the machining operation can be evaluated in real time. For this experiment, in addition to those already reported machining parameters, it was adopted advance of 0.1 mm/rev, average cutting speed of 67 m/min, variable cutting depth, according to the workpiece section, and rotation of 710 rpm.

For cutting temperature measurement, a digital infrared thermometer was used, and a measurement technique already established in the literature [7, 8, 47] coupled to a computer running data acquisition software was applied. The thermometer was always directed to the cutting area, as shown in Figure 3(b), in a distance of about 800 mm thereof. The infrared thermometer used allowed the cutting temperature measurement along the necking tests.

During the necking experiments, the obtained temperatures were collected throughout the process with an average of 15.6 points per second. Thus, a treatment for eliminating noise arising from distance and vibration of the thermometer was carried out in such way that a cutting temperature profile versus time could be obtained, for each necking. Also with these values, it was possible to obtain the maximum heating rates for each necking, which is the ratio of the difference between the maximum temperature

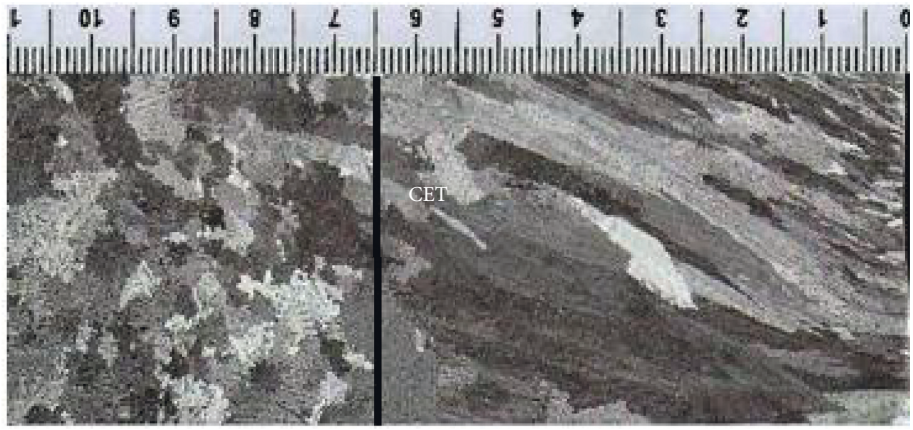

Figure 2: Solidification macrostructure with CET position.

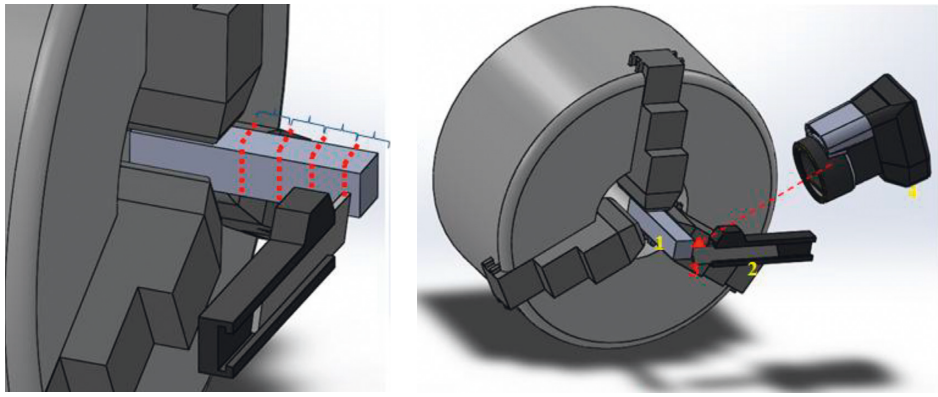

(a) (b)

Figure 3: (a) Schematic representation of the necking process and the divisions of the workpiece. (b) Schematic representation of the temperature acquisition region, where 1 is the workpiece, 2 is the chisel, 3 is the acquisition region, and 4 is the infrared thermometer.

Table 1: Position ranges from metal/mold interface of each necking.

Necking	Range measurements
1	0 to 10 mm
2	11 to 20 mm
3	21 to 30 mm
4	31 to 40 mm
5	41 to 60 mm
6	61 to 80 mm

reached and the initial temperature and the difference between the corresponding times in these temperatures.

For both visual and metric wear analysis, an optical stereomicroscopy was primarily used, in which the chisel images were made at a magnification of 20x, right after necking. After this, measurements were made with ImageJ® analysis software by drawing parallel lines to the reference cut edges and then drawing perpendicular lines from the reference to the point to be measured. With this technique several flank wear measurements of each sample were made. For the tool end of life criteria, it was considered the end of the experiment with wear value obtained the maximum flank wear (V_{BMAX}) in accordance with ISO 3685 [48].

All treatments and compiling data, consolidated in the form of graphs and expressions, carried out during this study were obtained through OriginPro 9.1® software.

3. Results and Discussion

3.1. Dependence of λ_2 on Solidification Thermal Parameters. Figures 4(a)–4(c) show experimental results of λ_2 versus position from metal/mold interface, growth rate, and cooling rate obtained for the investigated alloy studied in this work. It can be noted from Figure 4(a) that the experimental values of λ_2 increase progressively to furthest positions of the heat-extracting surface. Concurrent analysis of Figures 1(b) and (2) allows observing that the action of the cooling fluid requires growth and cooling rate values quite high near the metal/mold interface, and these thermal parameters gradually decrease during solidification due to the increased thermal resistance promoted by progressive formation of solid metal. This effect directly affects the side branches, increasing λ_2 values for more distant positions from the chilled interface.

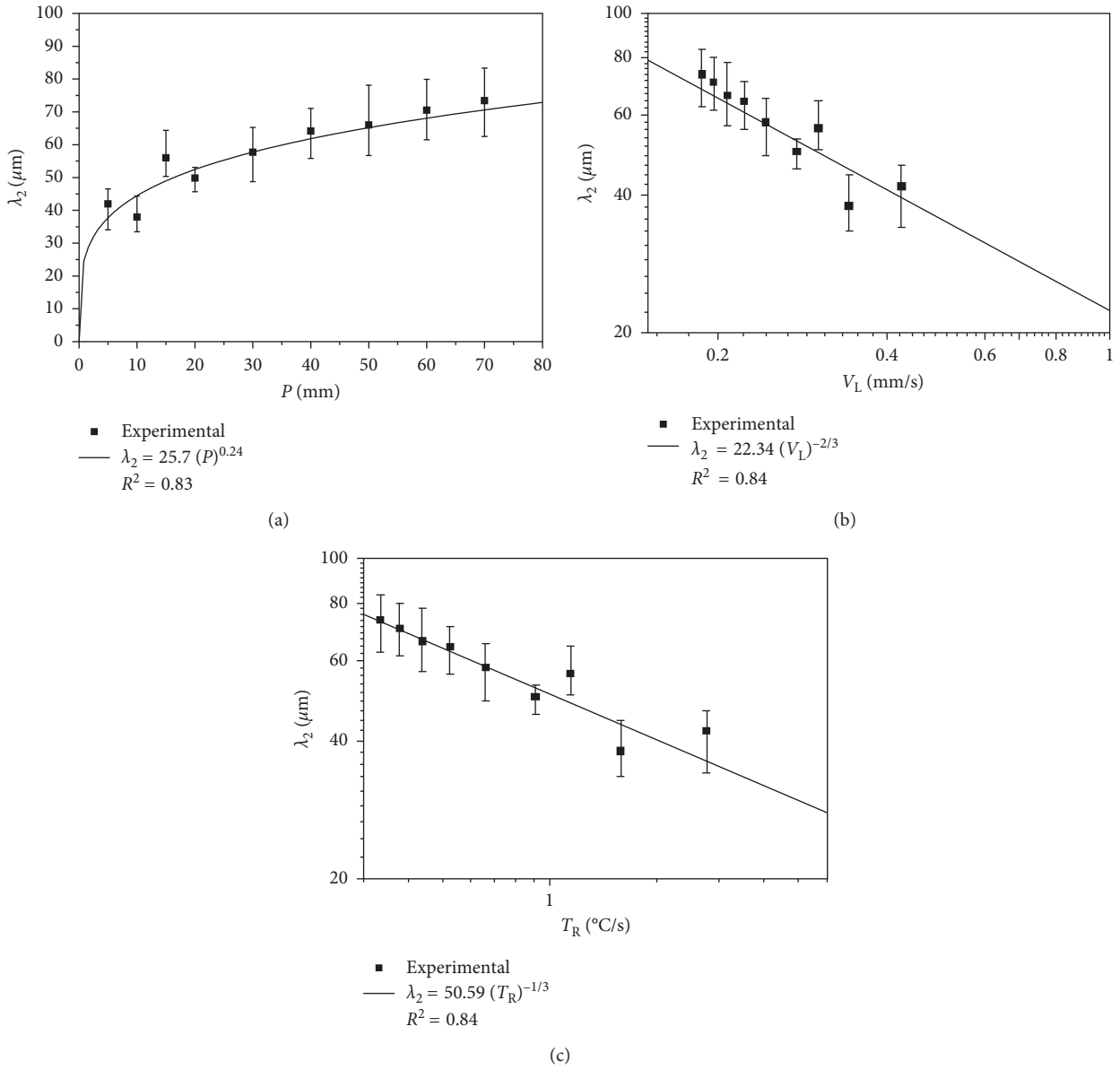

Figure 4: Experimental secondary dendrite arm spacings for the analyzed alloy as a function of (a) position, (b) growth rate, and (c) cooling rate.

3.2. Cutting Temperature Behavior. Figure 5(a) shows the results of temperature versus time for the six necking tests performed. It is observed, in all cases, a significant temperature increase followed by a slight decrease at the end of the process. Such results are already known from the literature [8], and probable reasons are that close to the end of the cutting area a smaller amount of heat is dissipated and because of the progressive increase tool wear along each assay [47]. It can also be seen that on the first three experiments, necking time was approximately the same, increasing on the two following neckings and decreasing on the last one.

Also in Figure 5(a), it is observed a significant increase in the maximum necking temperature reached furthest positions of the metal/mold interface, except for the last one where there has been a slight decrease in necking in relation to the previous position. This is due to this region that comprises part of the CET which, as a structural transition region, has a different behavior. The decrease on maximum necking temperature on the CET region was also found by Silva and coauthors, who analyzed the influence of the macrostructure on cutting temperatures of a directionally solidified Al–7 wt% Si alloy [41]. By observing Figures 4 and 5, it can be inferred that the cutting temperature increases with decreasing of both growth rate and cooling rate throughout the ingot, probably because of the largest amount dendritic arms formed.

In order to establish a relationship between the secondary dendrite arm spacing and cutting temperature, Figure 5(b) shows the maximum heating rates as a function of λ_2, considering only points where the directionality was observed (columnar zone). It is noted that the maximum

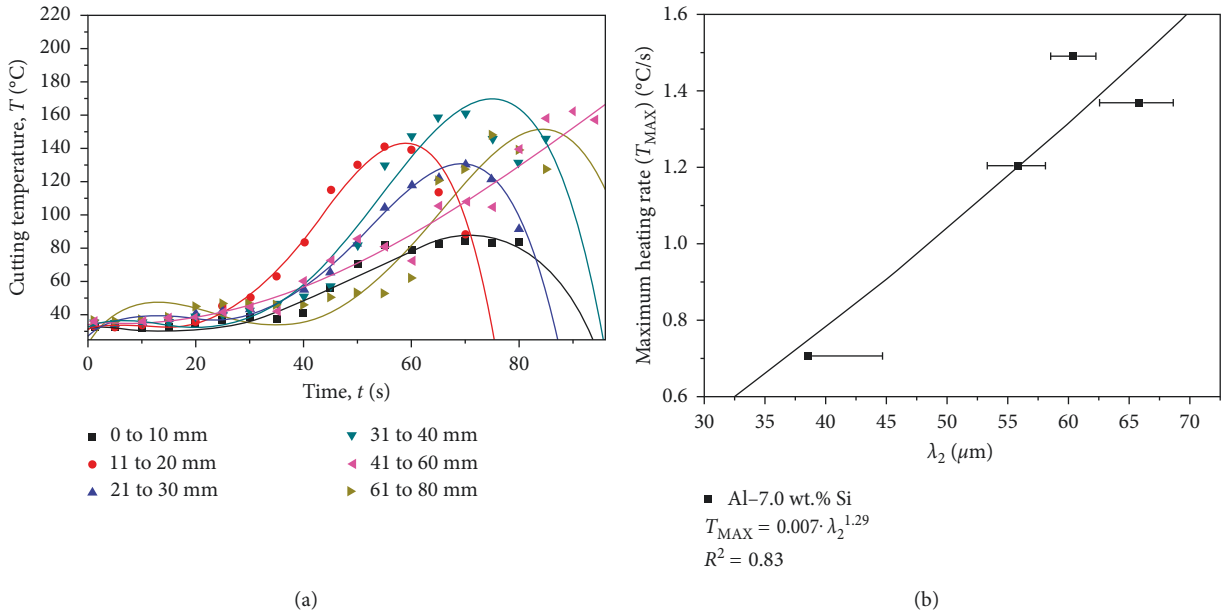

(a) (b)

Figure 5: (a) Temperature versus time for the six neckings. (b) Maximum heating rate as a function of secondary dendrite arm spacings.

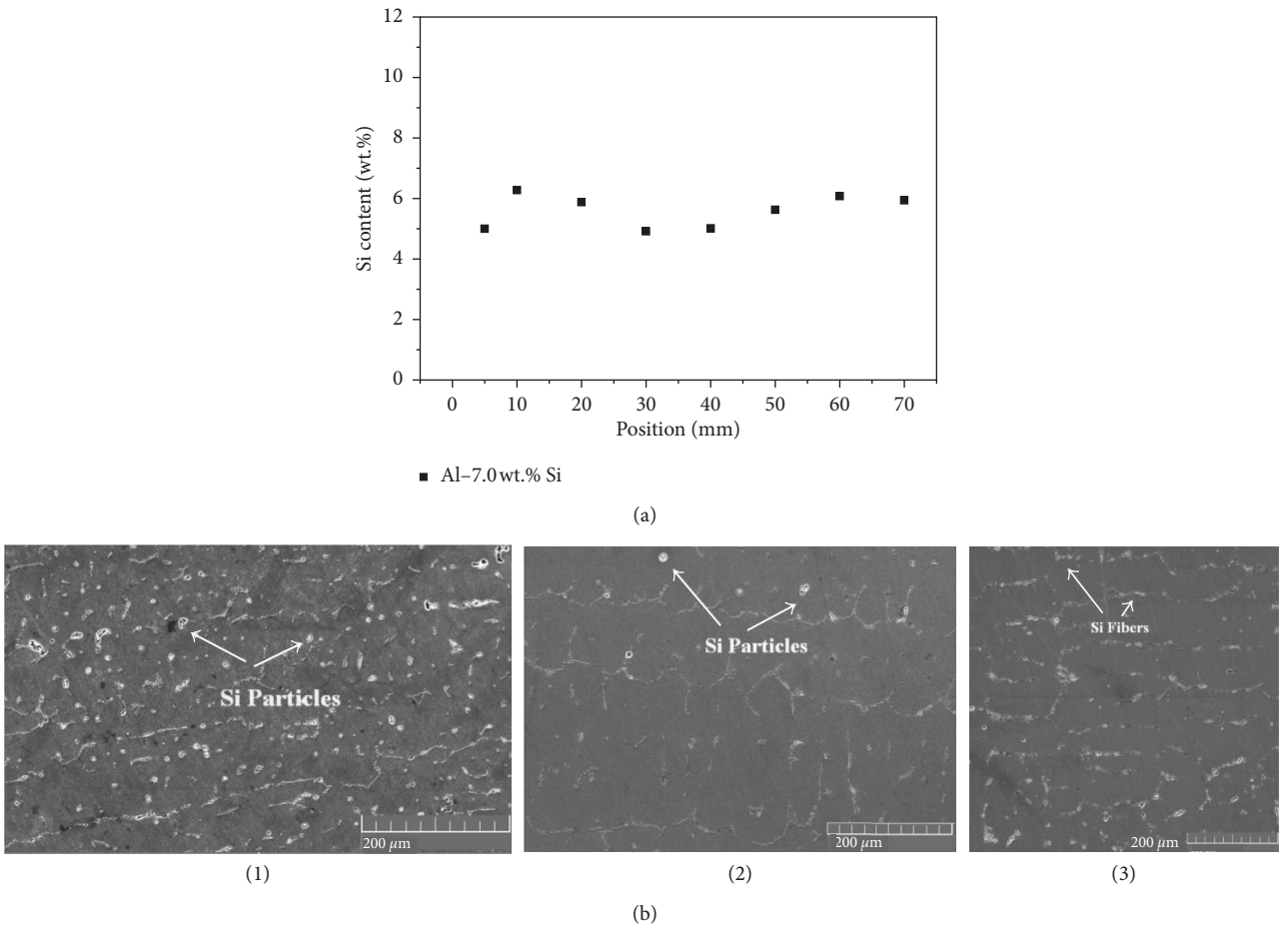

(a)

(1) (2) (3)

(b)

Figure 6: (a) Si segregation profile. (b) Morphology of Si along the ingot: (1) $P = 4$ mm, (2) $P = 30$ mm, and (3) $P = 50$ mm.

heating rate increases with increasing dendrite spacing whose relationship can be represented by a power function type with an efficient correlation coefficient.

3.3. Role of Si Morphology on Machinability. It is well known that a number of studies have showed that finer structures, that is, smaller dendrite arm spacings, have higher

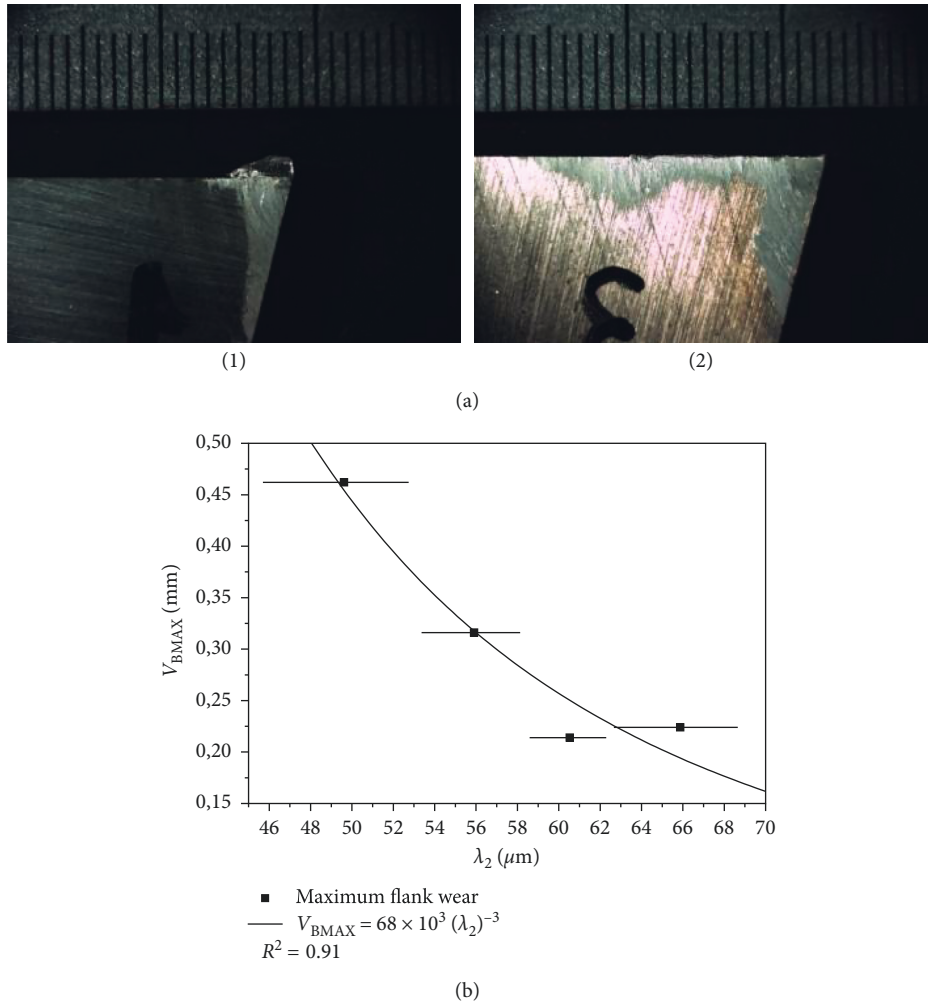

Figure 7: (a) Image of different tools used on necking tests: (1) before and (2) after removing false edge, showing flank wear. (b) Maximum flank wear as a function of secondary dendrite arm spacings.

mechanical properties such as tensile strength and hardness, decreasing the machinability of a material, that is, increasing efforts and consequently cutting temperature, but this is not the only factor that should be taken into account [23, 32, 44, 45]. Gandini et al. [32] who studied the effects of microstructure and hardness of hypoeutectic Al–Si alloys over their machinability found that finer as-cast microstructure requires maximum cutting force, and higher values for interdendritic spacing clearly reduce this demand. Si segregation profile and morphology of eutectic Si along the ingot, for instance, should be also analyzed. Silicon is an element that causes hardening of the alloy and the fragility of the chip, causing breakage [11]. Thus, despite the larger dendrite spacing inducing a tendency of reducing the cutting forces and the absence of significant Si segregation to furthest positions of the ingot, it can be observed by SEM images the increase of Si particles diameter beyond the transition from particles to fibers from 50 mm from the metal/mold interface, as shown in Figure 6. The increase of Si particle diameter in the outermost regions of the ingot base results in hardening of the alloy, as well as the morphology transition, once fibers have greater hardness than particles, increasing efforts and therefore the temperature cutting.

3.4. Tool Wear Behavior. Figure 7(a) shows the tips of one of the tools used during experiments (side view, by the flank) after necking. A false edge can be noted on image 1, which was found also in all tests performed. These false edges were immediately removed after neckings, such that the tool wear could be measured, with exception of the first necking, whose welding was so strong that it could not be removed. The observation of the images shows that there is a predominance of the tool flank wear.

The temperatures generated during the necking process without cutting fluid of a workpiece consisting of an aluminum alloy, probably contribute to the false edge, that stand out and inhibit more evident wear. The wear observed, therefore, may have been originated by the combination of two mechanisms: attrition and/or abrasion. The first one occurs when there is the formation of false cutting edge, interrupted

Table 2: Maximum tool wear in each necking position.

Maximum flank wear, V_{BMAX} (mm)	Positions (mm)
0.25	0 to 10
0.462	11 to 20
0.316	21 to 30
0.214	31 to 40
0.224	41 to 60
0.63	61 to 80

cuts, variable cutting depth, and vibration in the process, among others [9]. In this case, the formation of the false edge along the workpiece geometry (rectangular) may have been because of some of these factors which had favored the mechanism. The second one occurs when machining materials with high concentrations of very hard particles which encounter the surface of the tool during machining and during removal of the material by microgroovement, microcut, and microchipping [9]. In this case, the rotation slightly higher than the recommended (by limitations of equipment rotations range) and the fact that necking process requires a continuous effort of cutting tool, along with the presence of a highly abrasive alloying element on composition of workpiece (silicon—although in hypoeutectic composition), led to disruption in the formation of false edges initially formed.

According to ISO 3685 [48], the tool life is the time that it works effectively until losing their cutting capacity, within a previously established criteria. For the tool in question, it indicates as one of the criteria of the turning tool, the maximum tool wear $V_{BMAX} = 0.6$ mm, considering irregular wear. The lower values have found tool wear on neckings 1 to 5, as shown in Table 2, indicate that the end of tool life was not achieved in these cases despite necking process had occurred under severe conditions. These results can be explained by the fact that the piece machined is made of an aluminum alloy (a soft material, although having silicon in its composition) and the elements of tool composition that increase hot hardness and reduce wear. For the sixth test, it was observed that the end of tool life has been reached, which may be justified by that necking was performed at the CET region, a structural transition where coexist columnar and equiaxed grains randomly distributed.

In order to establish a relationship between the tool wear and the secondary dendrite arm spacing, Figure 7(b) shows the maximum wear found for each necking, due to λ_2, except for the first and sixth tests. In the first case, as the false edge could not be removed, this point was overlooked, and in the second case, the necking was carried out in a region where its directionality was not observed (CET position) and cannot be compared with tests in which necking was performed at the columnar region. It can be seen that tool wear decreases with increasing the secondary dendrite spacing and the relationship could be represented by a power-type function. This analysis complements the ones found for cutting temperature, which have showed higher cutting temperatures to positions furthest from the base of ingot and larger dendritic spacing. Higher cutting temperatures in an aluminum alloy cause an increased amount of false edge, reducing tool wear, as have been found in this study. Erstwhile, it was assumed that the fake edge protected the edge of the tool against wear and improved cutting by forming a more acute wedge angle. It is now known that the false edge is not a sharp edge, but a rounded mound of several thin and overlapped layers of material torn from the chip, generating a deterioration in the surface quality of the machined workpiece [49]; however, somehow it serves as protection to the cutting tool, avoiding excessive wear under severe conditions.

4. Conclusions

The following major conclusions are derived from the present study:

(1) Under unsteady-state conditions, secondary dendrite arm spacings (λ_2) were observed to increase with increasing of position from metal/mold interface and decrease with the increasing of the thermal parameters (V_L: growth rate and T_R: cooling rate).

(2) Experimental laws were obtained on the columnar zone for the maximum heating rate (T_{MAX}) and tool wear (V_{BMAX}) as functions of secondary dendrite spacing, $T_{MAX} = 0.007\ (\lambda_2)^{1.29}$ and $V_{BMAX} = 68 \times 10^3\ (\lambda_2)^{-3}$, respectively.

(3) Although the larger dendrite spacing induces a tendency of reducing the cutting forces and the absence of significant Si segregation to furthest positions of the ingot, the change of silicon morphology from particles to fibers and the increase of the particle size promoted the increasing of maximum heating rate for furthest positions from metal/mold interface.

(4) Machinability is a qualitative parameter and can change according to the criteria assumed for analysis. Thus, considering the results of cutting temperature (which is related to cutting forces), it is observed that the machinability of Al–7 wt.% Si alloy with an HSS T6 tool is higher for higher cooling rates (more refined dendritic spacing and smaller Si particle diameters), even though tool wear is higher, because the tool life was not reached in these cases. If tool wear is taken into account, for a roughing operation, which is the case of this work and the formation of the false edge does not detract from the dimensional tolerance, machinability is higher for lower cooling rates.

(5) On these cases, the region in which necking comprises parts of the CET was excluded of the aforementioned results, because as a structural transition region, it has a different behavior. Besides the maximum necking temperature reached did not follow the tendency of increase with the position from the metal/mold interface, the end of the tool life has been reached.

Conflicts of Interest

The authors declare that they have no conflicts of interest.

Acknowledgments

The authors acknowledge the financial support provided by IFPA (Federal Institute of Education, Science and Technology of Pará), UFPA (Federal University of Pará), CAPES (Coordination of Superior Level Staff Improvement), and CNPq (The Brazilian Research Council), Brazil.

References

[1] F. R. Faustino, J. O. Santos, and I. F. Machado, *Método para ensaios de avaliação de usinabilidade de materiais metálicos utilizando torno CNC e torno convencional (mecânico), in VIII Encontro de Iniciação Científica do LFS*, 2007.

[2] M. B. Tessler and C. A. Barbosa, "A usinabilidade dos aços inoxidáveis," *Metalurgia e Materiais*, vol. 49, no. 413, pp. 32–41, 1993.

[3] D. O'Sullivan and M. Cotterell, "Temperature measurement in single point turning," *Journal of Materials Processing Technology*, vol. 118, no. 1–3, pp. 301–308, 2001.

[4] F. W. Taylor, "On the art of cutting metals," *ASME Transactions*, vol. 28, p. 31, 1907.

[5] K. J. Trigger and B. T. Chao, "An analytical evaluation of metal-cutting temperatures," *ASME Transactions*, vol. 78, p. 57, 1951.

[6] M. A. Taha, N. A. El-Mahallawy, R. M. Hammouda, T. M. Moussa, and M. H. Gheith, "Machinability characteristics of lead free-silicon brass alloys as correlated with microstructure and mechanical properties," *Ain Shams Engineering Journal*, vol. 3, no. 4, pp. 383–392, 2012.

[7] M. A. Davies, T. Ueda, R. M'Saoubi, B. Mullany, and A. L. Cooke, "On the measurement of temperature in material removal processes," *CIRP Annals*, vol. 56, no. 2, pp. 581–604, 2007.

[8] N. A. Abukhshim, P. T. Mativenga, and M. A. Sheikh, "Heat generation and temperature prediction in metal cutting: a review and implications for high speed machining," *International Journal of Machine Tools and Manufacture*, vol. 46, no. 7-8, pp. 782–800, 2006.

[9] U. B. Souto, *Monitoramento do Desgaste de Ferramenta no Processo de Fresamento Via Emissão Acústica*, Universidade Federal de Uberlândia, Uberlândia, MG, Brazil, 2007.

[10] R. M. U. Nogueira, *Obtenção e Estudo de Insertos Sinterizados de Aços Rápidos AISI M2, M3/2 E T15*, UDESC, Joinville, SC, Brazil, 2004.

[11] D. W. Hetzner, "Refining carbide size distributions in M1 high speed steel by processing and alloying," *Materials Characterization*, vol. 46, no. 2-3, pp. 175–182, 2001.

[12] E. M. Trent and P. K. Wright, *Metal Cutting*, Butterworth-Heineman, Boston, MA, USA, 2000.

[13] C. Zimmerman, S. P. Boppana, and K. Katbi, "Machinability test methods," in *ASM Metals Handbook*, vol. 10, ASM International, Metals Park, OH, USA, 1990.

[14] J. M. V. Quaresma, C. A. Santos, and A. Garcia, "Correlation between unsteady-state solidification conditions, dendrite spacings, and mechanical properties of Al-Cu alloys," *Metallurgical and Materials Transactions A*, vol. 31, no. 12, pp. 3167–3178, 2000.

[15] A. Bahmani, N. Hatami, N. Varahram, P. Davami, and M. O. Shabani, "A mathematical model for prediction of microporosity in aluminum alloy A356," *International Journal of Advanced Manufacturing Technology*, vol. 64, no. 9–12, pp. 1313–1321, 2013.

[16] T. A. Costa, A. L. Moreira, D. J. Mooutinho et al., "Growth direction and Si alloying affecting directionally solidified structures of Al–Cu–Si alloys," *Materials Science and Technology*, vol. 31, no. 9, pp. 1103–1112, 2015.

[17] E. C. Araújo, A. S. Barros, R. H. Kikuchi et al., "The role of Si and Cu alloying elements on the dendritic growth and microhardness in horizontally solidified binary and multicomponent aluminum-based alloys," *Metallurgical and Materials Transactions A*, vol. 48, no. 3, pp. 1163–1175, 2017.

[18] G. R. Santos, D. D. Costa, F. L. Amorim, and R. D. Torres, "Characterization of DLC thin film and evaluation of machining forces using coated inserts in turning of Al–Si alloys," *Surface and Coatings Technology*, vol. 202, no. 4–7, pp. 1029–1033, 2007.

[19] H. Ye, "An overview of the development of Al-Si-alloy based material for engine applications," *Journal of Materials Engineering and Performance*, vol. 12, no. 3, pp. 288–297, 2003.

[20] A. Bahmania, G. B. Eisaabadi, P. Davamia, N. Varahrama, and M. O. Shabanid, "Effects of hydrogen level and cooling rate on ultimate tensile strength of Al A319 alloy," *Russian Journal of Non-Ferrous Metals*, vol. 55, no. 4, pp. 365–370, 2014.

[21] Y. Wang, B. Liu, J. Song, X. Yang, and K. Wu, *Advanced Materials Research*, vol. 381, p. 16, 2012.

[22] M. O. Shabani and A. Mazahery, "Prediction of mechanical properties of cast A356 alloy as a function of microstructure and cooling rate," *Archives of Metallurgy and Materials*, vol. 56, no. 3, p. 671, 2011.

[23] A. Mazahery and M. O. Shabani, "Modification mechanism and microstructural characteristics of eutectic Si in casting Al-Si alloys: a review on experimental and numerical studies," *Journal of the Minerals, Metals, and Materials Society*, vol. 66, no. 5, pp. 726–738, 2014.

[24] A. Mazahery and M. O. Shabani, "Process conditions optimization in Al–Cu alloy matrix composites," *Powder Technology*, vol. 225, pp. 101–106, 2012.

[25] M. O. Shabani and A. Mazahery, "Artificial Intelligence in numerical modeling of nano sized ceramic particulates reinforced metal matrix composites," *Applied Mathematical Modelling*, vol. 36, no. 11, pp. 5455–5465, 2012.

[26] M. O. Shabani and A. Mazahery, "Application of finite element model and artificial neural network in characterization of Al matrix nanocomposites using various training algorithms," *Metallurgical and Materials Transactions A*, vol. 43, no. 6, pp. 2158–2165, 2012.

[27] A. Mazahery and M. O. Shabani, "A356 reinforced with nanoparticles: numerical analysis of mechanical properties," *JOM*, vol. 64, no. 2, pp. 323–329, 2012.

[28] M. O. Shabani and A. Mazahery, "Optimization of process conditions in casting aluminum matrix composites via interconnection of artificial neurons and progressive solutions," *Ceramics International*, vol. 38, no. 6, pp. 4541–4547, 2012.

[29] M. O. Shabani and A. Mazahery, *Materials and Technology*, vol. 46, p. 2, 2012.

[30] S. Z. Lu and A. Hellawell, "The mechanism of silicon modification in aluminum-silicon alloys: impurity induced twinning," *Metallurgical Transactions A*, vol. 18, no. 10, pp. 1721–1733, 1987.

[31] N. R. Rathod and J. V. Manghani, "Effect of modifier and grain refiner on cast Al-7Si aluminum alloy: a review," *International Journal of Emerging Trends in Engineering and Development*, vol. 5, p. 574, 2012.

[32] E. T. S. Gandini, B. M. C. Donadoni, A. I. S. Antonialli, and J. E. Spinelli in *22nd International Congress of Mechanical Engineering (COBEM 2013)*, RibeirãoPreto, 2004.

[33] E. Çadirli, "Effect of solidification parameters on mechanical properties of directionally solidified Al-Rich Al-Cu alloys,"

Metals and Materials International, vol. 19, no. 3, pp. 411–422, 2013.

[34] H. Kaya, U. Boyuk, E. Çadirli, and N. Marasli, "Influence of growth rate on microstructure, microhardness, and electrical resistivity of directionally solidified Al-7 wt.% Ni hypo-eutectic alloy," *Metals and Materials International*, vol. 19, no. 1, pp. 39–44, 2013.

[35] D. M. Rosa, J. E. Spinelli, and A. Garcia, "Tertiary dendrite arm spacing during downward transient solidification of Al–Cu and Al–Si alloys," *Materials Letters*, vol. 60, no. 15, pp. 1871–1874, 2006.

[36] A. P. Silva, A. Garcia, and J. E. Spinelli, "Microstructure morphologies during the transient solidification of hypo-monotectic and monotectic Al–Pb alloys," *Journal of Alloys and Compounds*, vol. 509, no. 41, pp. 10098–10104, 2011.

[37] J. N. Silva, D. J. Moutinho, A. L. Moreira, I. L. Ferreira, and O. L. Rocha, "The columnar to equiaxed transition during the horizontal directional solidification of Sn–Pb alloys," *Journal of Alloys and Compounds*, vol. 478, no. 1-2, pp. 358–366, 2009.

[38] J. N. Silva, D. J. Moutinho, A. L. Moreira, I. L. Ferreira, and O. L. Rocha, "Determination of heat transfer coefficients at metal–mold interface during horizontal unsteady-state directional solidification of Sn–Pb alloys," *Materials Chemistry and Physics*, vol. 130, no. 1-2, pp. 179–185, 2011.

[39] J. H. Sokołowski, D. Szablewski, W. Kasprzak, E. G. Ng, and M. Dumi-Trescu, *Journal of Achievements in Materials and Manufacturing Engineering*, vol. 17, p. 15, 2006.

[40] Y. Zedan, F. H. Samuel, A. M. Samuel, and H. W. Doty, "Effects of Fe intermetallics on the machinability of heat-treated Al–(7–11)% Si alloys," *Journal of Materials Processing Technology*, vol. 210, no. 2, pp. 245–257, 2010.

[41] A. P. Silva, I. R. Prado, J. S. Barros, C. A. P. Silva, A. L. Moreira, and O. L. Rocha, "Influence of growth rate on microstructure, microhardness, and electrical resistivity of directionally solidified Al-7 wt.% Ni hypo-eutectic alloy," *Defect and Diffusion Forum*, vol. 365, pp. 116–121, 2015.

[42] D. B. Carvalho, A. L. Moreira, D. J. Moutinho, J. M. Filho, O. L. Rocha, and J. E. Spinelli, "The columnar to equiaxed transition of horizontal unsteady-state directionally solidified Al-Si alloys," *Materials Research*, vol. 17, no. 2, pp. 498–510, 2014.

[43] D. B. Carvalho, T. A. Costa, A. L. Moreira et al., "Solidification thermal parameters and dendritic growth during the horizontal directional solidification of Al-7wt.%Si alloy," *Revista Escola de Minas*, vol. 67, no. 3, pp. 265–270, 2014.

[44] M. D. Peres, C. A. Siqueira, and A. Garcia, "Macrostructural and microstructural development in Al–Si alloys directionally solidified under unsteady-state conditions," *Journal of Alloys and Compounds*, vol. 381, no. 1-2, pp. 168–181, 2004.

[45] O. L. Rocha, C. A. Siqueira, and A. Garcia, "Cellular spacings in unsteady-state directionally solidified Sn–Pb alloys," *Materials Science and Engineering: A*, vol. 361, no. 1-2, pp. 111–118, 2003.

[46] A. R. Machado, A. M. Abrão, R. T. Coelho, and M. B. Silva, *Teoria da Usinagem dos Materiais*, Edgard Blucher, Jardim Paulista, SP, Brazil, 2011.

[47] M. B. Silva and J. Wallbank, "Cutting temperature: prediction and measurement methods—a review," *Journal of Materials Processing Technology*, vol. 88, no. 1–3, pp. 195–202, 1999.

[48] ISO 3685, *Tool-Life Testing with Single-Point Turning Tools*, 1993.

[49] B. Haddag and M. Nouari, "Tool wear and heat transfer analyses in dry machining based on multi-steps numerical modelling and experimental validation," *Wear*, vol. 302, no. 1-2, pp. 1158–1170, 2013.